Impact of proton irradiation on photoluminescent properties of C-doped ZrO2 films prepared by ALD

Applied Surface Science

Impact of proton irradiation on photoluminescent properties of C-doped ZrO2 films prepared by ALD

--Manuscript Draft--

Manuscript Number:	
Article Type:	Full Length Article
Keywords:	Optical coatings Space radiation Photoluminescence Oxide
Corresponding Author:	Anna Sytchkova Rome, RM ITALY
First Author:	Anna Sytchkova
Order of Authors:	Anna Sytchkova
	Maria Lucia Protopapa
	Emiliano Burresi
	Paolo Olivero
	Toni Dunatov
	Hristo Kolev
	Zdravko Siketic
	Leander TAPFER
	Zhihao Wang
	Hongbo He
	Yanzhi Wang
Abstract:	Amorphous C-doped zirconia thin films grown by ALD technique on fused silica substrates have high transmittance and significant photoluminescence (PL) capacity suitable for application as a transparent material to convert high energy into lower energy photons as well as an optical sensor of radiation. Due to carbon doping, zirconia films present three main PL transitions: Transition I and II at λem=450 nm (λexc =200 and 270 nm), related to sp3 and sp2 C-C bonds, and Transition II at λem=450 nm (λexc=300 nm) that can be assigned to C=O bonds which introduce n levels in the π- π* gap. Protons with energy of 100 keV and two values of fluence (1•1012 and 5•1014 p+/cm2) were used to modify the film properties. The changes induced by the radiation in the chemical composition of the films have been monitored as a function of irradiation dose using in-depth resolved XPS analysis. We demonstrate that C-Zr bonds are cleaved by protonation in favor of Zr-O, C-H and C=O bonds. As a consequence, more defect levels are formed in the π- π* gap of C. Consequently, the emission due to Transitions I becomes more intense for high energy doses, getting intensity values close to Transitions I/II.
Suggested Reviewers:	Adriana Szeghalmi Adriana.Szeghalmi@iof.fraunhofer.de specialist in ALD coatings
	James Barrie James.D.Barrie@aero.org coatings for space applications
	Alexander Tikhonravov tikh@srcc.msu.ru expertize in optical coating design and characterization

Impact of proton irradiation on photoluminescent properties of C-doped ZrO_2 films prepared by ALD

Anna Sytchkova[a,*], Maria Lucia Protopapa[b,*], Emiliano Burresi[b], Paolo Olivero[c], Toni Dunatov[d], Hristo Kolev[e], Zdravko Siketić[d], Leander Tapfer[b], Zhihao Wang[f,g], Hongbo He[f,h], Yanzhi Wang[f]

[a] Optical Coatings Group, Department for Energy Technologies and Renewable Sources, ENEA C.R. Casaccia, via Anguillarese 301, Rome 00123, Italy
[b] Department for Sustainability, ENEA C.R. Brindisi, SS 7 Appia Km 706, 72100 Brindisi, Italy
[c] Physics Department and "NIS" inter-departmental centre, University of Torino, via P. Giuria 1, 10125 Torino, Italy
[d] Laboratory for ion beam interaction, Institut Ruđer Bosković, Bijenička cesta 54, 10000 Zagreb, Croatia
[e] Institute of Catalysis, Bulgarian Academy of Sciences, Acad. G. Bonchev St., Bldg. 11, 1113 Sofia, Bulgaria
[f] Laboratory of Thin Film Optics, Shanghai Institute of Optics and Fine Mechanics, No. 390 Qinghe Road, Jiading District, Shanghai 201800, China
[g] Center of Materials Science and Optoelectronics Engineering, University of Chinese Academy of Sciences, Beijing 100049, China
[h] Key Laboratory of Materials for High Power Laser, Shanghai Institute of Optics and Fine Mechanics, No. 390 Qinghe Road, Jiading District, Shanghai 201800, China

ARTICLEINFO

Keywords:
Optical coatings
Space radiation
Photoluminescence
Oxide

ABSTRACT

Amorphous C-doped zirconia thin films grown by ALD technique on fused silica substrates have high transmittance and significant photoluminescence (PL) capacity suitable for application as a transparent material to convert high energy into lower energy photons as well as an optical sensor of radiation. Due to carbon doping, zirconia films present three main PL transitions: Transition I and II at λ_{em}=450 nm (λ_{exc} =200 and 270 nm), related to sp^3 and sp^2 C-C bonds, and Transition II at λ_{em}=450 nm (λ_{exc}=300 nm) that can be assigned to C=O bonds which introduce n levels in the π- π* gap. Protons with energy of 100 keV and two values of fluence ($1\cdot10^{12}$ p+/cm^2 and $5\cdot10^{14}$ p+/cm^2) were used to modify the film properties. The changes induced by the radiation in the chemical composition of the films have been monitored as a function of irradiation dose using in-depth resolved XPS analysis which evidenced modification of C-Zr, Zr-O, C-H, C≡C and C=O bonds. We demonstrate that C-Zr bonds formed in the film depth are cleaved by protonation in favor of Zr-O, C-H and C=O bonds establishment. As a consequence, more defect levels are formed in the π- π* gap of carbon. Consequently, the emission due to Transitions I becomes more intense for high energy doses, getting intensity values close to Transitions I/II.

1. Introduction

Zirconium oxide (or zirconia, ZrO_2) manufactured using the atomic layer deposition (ALD) technique is a relatively uncommon thin film material for optical applications. ALD enables conformal coating of complicated surfaces and allows for atomic-scale engineering of materials and therefore, for an ideal process for engineering of the optical properties of coatings.[1]

For many applications, zirconia may be implemented in the form of coatings, which may be a single film or a multilayer. Zirconia-based coatings are widely used for electric insulation in semiconductor devices [2], or as thermal barriers [3]. Zirconia thin films also represent a way to nanosize the material, which may result in an advantageous strategy for many demanding applications where traditionally bulk or powder materials have been used. The optical properties of thin films are known to be conditioned by their structure and microstructure, both dependent on the manufacturing method and the deposition conditions. Common ways to manufacture thin films of zirconia are (magnetron) sputtering [4] and electron-beam evaporation [5], although pulsed laser deposition [6] and sol-gel technique [7] may also be implemented. When starting from a metallic target, zirconia may be obtained by either post-deposition thermal annealing of sputtered zirconium, or by adding oxygen to the working gas during the deposition (reactive sputtering). Any of the aforementioned deposition techniques can provide polycrystalline or amorphous zirconia films of various packing densities and optical properties. In [8] ultrathin (about 3 nm thick) zirconia films prepared by Atomic Layer Deposition (ALD) were studied as a novel high-k material for use in microelectronics. The films were investigated for stoichiometry and surface roughness with the main focus on their electrical characteristics.

Zirconia's remarkable catalytic properties [9] and chemical persistence are exploited in bio- and medical applications [10], and it is a promising solid electrolyte [11]. The particular combination of chemical, mechanical and optical properties characterizing this ceramic renders it quite unique for applications in particularly demanding fields like technologies for space and for nuclear energy [12]. For zirconium alloys used in corrosive and nuclear environments, zirconia is a protecting layer as it is exceptionally tolerant to radiation damage [13]. It is used in radiation dosimeters and devices for radiation imaging [14].

Among the properties of zirconia readily exploitable in optics are its high refractive index and significant luminescent yield [15]. Zirconia has three crystalline phases and both crystalline and amorphous zirconia coatings may be fabricated for specific applications. Stabilization and tuning of structural and hence mechanical and optical properties of zirconia is often used by doping with metals like Ce [16] and Er [17], or other ceramics like Y_2O_3 [18], CeO_2 [19], Fe_2O_3 and MnO_2 [20]. In particular, doping may be used to tune the luminescence properties of zirconia [21, 22].

Here we present a study on a set of C-doped amorphous thin films of zirconia manufactured by ALD for space applications. The films were prepared on fused silica substrates with a thickness of about 200 nm, which is relevant for many optical devices. Our recent study [23] reported characterization of these films in terms of their complex refractive index and its in-depth variation prior to and after irradiation with 100 keV protons.

This article reports on the composition and the photo-induced luminescence (PL) ability of C-doped a-ZrO_2 films. The origins of PL in zirconia is still a subject of debate [24-26]. Oxygen vacancies [27] as well as impurities, which are either deposition-dependent or absorbed upon exposure of the film to the environment [28, 29], are normally indicated as PL origins. It is also known that the PL of zirconia is affected by both temperature regime and energetic particle irradiation [25]. In this study we show that the pivotal mechanism of the PL in our C-doped a-ZrO_2 films is the interaction of carbon impurities and protons with over-stoichiometric oxygen and this mechanism may be influenced by low-energy protons. Modification of the PL of the films may find applications in dosimetry and radiation imaging.

*Corresponding authors at: Department for Energy Technologies and Renewable Sources, ENEA C.R. Casaccia, via Anguillarese 301, Rome 00123, Italy (Anna

Sytchkova) and Department for Sustainability, ENEA C.R. Brindisi, SS 7 Appia Km 706, 72100 Brindisi, Italy (Maria Lucia Protopapa)
E-mail address: anna.sytchkova@enea.it (Anna Sytchkova) and lucia.protopapa@enea.it (Maria Lucia Protopapa)

2. Experimental details

2.1. Sample manufacturing and irradiation

Zirconia films were deposited using an R-200 Advanced system by Picosun Oy, on 3 mm thick fused silica and 0.5 mm thick crystalline silicon substrates. The deposition for 2000 cycles was performed using Tetrakis zirconium $C_8H_{24}N_4Zr$ as precursor at 700 Pa pressure and the substrate temperature of 150 °C. The chosen deposition conditions assured a relevant carbon doping level via a slightly incomplete chemical reaction towards the sample surface. As carbon doping on zirconia was obtained through incomplete chemical reaction at the last stage of the film growth, the film resulted inhomogeneous in its upper 5% of thickness, approximately. TEM analysis performed using a FEI Talos F200 (Thermo Fisher) microscope confirmed the amorphous structure of the coatings and revealed no carbon agglomerates in the films, Fig.1a. Notice that the gradient layer between the Si substrate and the film evidenced in the figure, is composed mostly of the native silicon oxide covered with first atomic strata of zirconia. The results of ellipsometric and X-ray reflectometry analyses [23, 30] revealed the in-depth inhomogeneity of the film material. All films can be modeled as bilayers, Fig.1b, being the part near the substrate optically denser. The relatively thin upper part of all films (about 10 nm) has a lower refractive index and a higher extinction coefficient due to a higher amount of residual organic impurities.

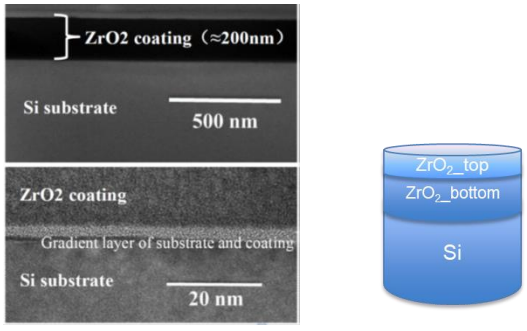

Fig. 1 Cross-section TEM image of zirconia film deposited on silicon substrate (a). Enlarged TEM image showing the microstructure of the interface gradient layer between zirconia coating and silicon substrate (b). Schematic representation of the zirconia film modeled as a bilayer of an optically denser bottom layer and a less dense top (upper) layer (c).

The samples deposited on fused silica were organized in two groups which differed by the amount of the residual organic substance in the upper part of the film: the samples 7A, 8A and 9A were richer in doping material in their thicker upper layer, while the samples 10A, 11A and 12A had thinner upper layer with less doping. [30]

The samples were then irradiated by low-energy protons (100 keV) at fluence ranging from $1{\cdot}10^{12}$ p^+/cm^2 through $5{\cdot}10^{14}$ p^+/cm^2, Tab. 1, repeating the irradiation conditions for each of two groups of samples. The irradiation was conducted at the DiFU beamline of the Laboratory for ion beam interactions, RBI. A 100 keV proton beam was obtained using the 1 MV electrostatic Tandetron accelerator with a terminal voltage of 50 kV. Prior to irradiation, the chamber was evacuated down to $5{\cdot}10^{-6}$ - $5{\cdot}10^{-7}$ mbar. The beam was scanned over the sample using electrostatic scanners in order to homogenize the dose, and the current was monitored with periodic Faraday cup insertions, as well as readings from slits touching the outside of the beam. The area scanned is defined by the slits and was set to 1 x 1.5 cm^2, and 1.5 x.1.5 cm^2, depending on the sample.

Table 1
Irradiation parameters for the investigated samples.

Sample	Fluence (p^+/cm^2)	Average rate (p^+/cm^2 s)
7A	1,00E+12	1,67E+10
10A	1,00E+12	1,67E+10
8A	2,00E+13	1,08E+10
11A	2,00E+13	1,04E+10
11B	4,50E+12	1,08E+10
9A	5,00E+14	1,12E+11
12A	5,00E+14	2,04E+10
FS A	1,00E+12	1,71E+10
FS B	5,00E+14	6,81E+10

2.2. Characterization techniques

Optical, microstructural and compositional properties of the C-doped zirconia samples have been thoroughly investigated before and after proton irradiation and reported in our previous publication [23].

XPS data for pristine and for irradiated samples were acquired by Thermo Fisher K-Alpha spectrometer using only its AlKα monochromated X-ray source (1486.6 eV). The chemical composition of the films was studied for the film surface and in-depth profile. The XPS measurements were collected for C1s, O1s and Zr3d core levels at three different depths of the film, which were achieved after 600 s, 1200 s and 1740 s of sputtering with Ar+ ions, respectively. These sputtering times correspond, approximately, to 60 nm from the surface (or 1/3 of the film thickness), to 120 nm from the surface (2/3 of film thickness) and to 170 nm from the surface, which is almost at the film bottom.

Photo-induced luminescence was measured by a FluoroMax 4 spectrofluorometer (Horiba Jobin Yvon, Edison, NJ, USA). Adjustment of the position of the sample was necessary in order to get an incidence angle of 30°.

3. Characterization results and discussion

3.1. XPS analysis

The XPS spectra were analyzed using SpecsLab2 CasaXPS software (Casa Software Ltd). The processing includes subtraction of Shirley-type background [31]. The fitting of peak profiles (both spectral positions and areas) was performed using symmetrical Gaussian-Lorentzian approximation. The relative concentrations of the investigated chemical species were determined through normalization of the peak areas to their photoionization cross-sections calculated using Scofield formula [32].

For Zr3d band, high resolution XP spectra taken on the pristine ZrO_2 sample reveal main peaks whose values of binding energy (181.9 eV) are typical for ZrO_2 on the film surface, while they are shifted (+0.1-0.3 eV) for the three depths inside the film, Fig.2a. As a result of the fitting procedure, it was obtained that the XPS signal is attributable in large part to the maximum coordination for zirconium (Zr^{4+}) with the presence of a specie indicated as Zr-C whose binding energy is positioned between that of metallic Zr (positioned around 180.0-180.9 eV) and that relative to Zr^{4+}. Hence, the broad peaks marked as Zr-C and colored in blue are assigned to zirconium bonded to the carbon atom. Due to the lower electronegativity of carbon with respect to oxygen, the $Zr3d_{5/2}$ core level binding energy is lower for zirconium atoms bonded to carbon atoms with respect to zirconium atoms bonded to oxygen. For each sample analyzed, no sub-oxides compounds like Zr_2O_3 and ZrO were detected. It means that the ZrO_2 is the predominant oxidized specie [33].

The presence of the zirconium carbide in the film is confirmed by the C≡C bond signal revealed on C1s core level band acquired at internal levels of the film and reported in Fig. 2b (peaks marked with blue color). Besides the Zr-C bond, three components were used to fit the XPS signal for the C1s band, being the first corresponding to the carbonate bond C=O (peaks marked in purple), which is higher for the sample surface due to environmental contamination. The second component corresponds to the oxygen bond C-O and indicates presence of HCO species (peaks marked in orange). The third corresponds to the C-C bond, which overlaps with hydrocarbon bond C-H (peaks marked in green). Only three contributions

were employed to fit the C1s band at the top of the film as Zr-C bond signal was absent in that spectrum, supporting the aforementioned analysis of Zr3d band.

In the O1s band, a contribution assigned to the O-H bond was included, Fig. 2c. This signal encloses the *Oad* chemisorbed contribution, so-called non-lattice oxygen [33]. These volatile species are weakly bonded and hence, the decrease of this peak may be partially due to the sputtering of the sample performed for the in-depth analysis.

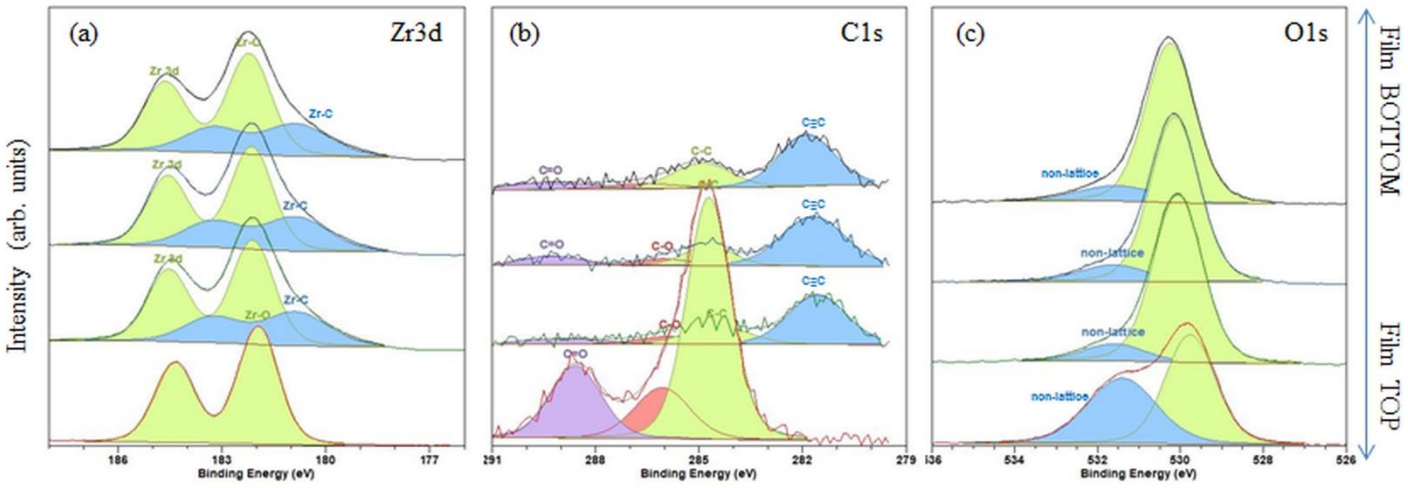

Pristine			Non-Lattice	Zr-O	Zr-C				
sputt.time		O 1s	O 1s (Non-Lattice)	Zr 3d (Zr-O)	Zr 3d (Zr-C)	C≡C	C-C	C-O	C=O
0s	at. %	37,52	31	11,15			12,66	3,31	4,37
600s	at. %	66,6	8,43	12,08	5,81	4	1,64	0,76	0,68
1200s	at. %	65,56	9,36	11,98	6,03	4,46	1,4	0,47	0,74
1740s	at. %	64,43	10,09	12,21	5,73	4,07	2,07	0,53	0,86

Fig. 2 Evolution of the high-resolution XP spectra of core levels of Zr3d (a), C1s (b) and O1s (c) along the thickness of a pristine ZrO_2 film.

After the proton irradiation, for all our samples, a general decrease of the intensity (and area) ratio was observed for the Zr-C bond signal in Zr3d band and for the C≡C bond signal in C1s band. In particular, this effect is more evident for samples 9A and 12A (fluence of $5 \cdot 10^{14}$ p^+/cm^2), along the entire film thickness but especially at the film bottom, whereas this ratio is slightly lower for the samples irradiated at lower dose (7A and 10A, fluence $1 \cdot 10^{12}$ p^+/cm^2). In particular, for sample 7A and 10A, protonation induced an increase of the C-C/C-H signal with respect to Zr-C exclusively at the top layer of the film, i.e. at 1/3 of the film thickness (60 nm). Conversely, for the samples 7 and 9 with initially higher amounts of non-lattice oxygen (higher O-H bond signal in O1s band and C-O bond in C1s band) this signal further increases upon irradiation and is further homogenized along all the film thickness with the dose increase. This effect is much less expressed for the samples 10A and 12A with initially lower content of non-lattice oxygen. Therefore, we infer that protonation induces cleavage of C≡C bonds and, depending on the sample C-doping level (connected to the initial amount of non-lattice oxygen), this cleavage may induce formation of C=O and C-C/C-H bonds. The homogenization of the signal related to these bonds is determined by the increase of the irradiation effect along the distance from the sample surface which compensates the initial inhomogeneity of the film material. Formation of carbonates and hydrocabonates at the expense of carbide is hence an effect of protonation of our ZrO_2 films. This effect is less pronounced for the samples initially poorer in doping material and in non-lattice oxygen.

Sample 7A			Non-Lattice	Zr-O	Zr-C				
sputt.time		O 1s	O 1s (Non-Lattice)	Zr 3d (Zr-O)	Zr 3d (Zr-C)	C≡C	C-C	C-O	C=O
600s	at. %	65,11	10,05	12,64	4,92	3,53	1,76	0,86	1,13
1200s	at. %	67,32	9,27	12,07	5,46	3,33	1,49	0,76	0,29
1740s	at. %	67,91	8,2	12,14	5,3	3,88	1,46	0,78	0,33

Sample 10A								
sputt.time	O 1s	O 1s (Non-Lattice)	Zr 3d (Zr-O)	Zr 3d (Zr-C)	C≡C	C-C	C-O	C=O
600s	66,99	8,44	12,12	5,31	3,71	1,91	0,56	0,96
1200s	66,27	9,51	11,48	5,58	3,32	2,29	0,81	0,74

Sample 9A			Non-Lattice	Zr-O	Zr-C				
sputt.time		O 1s	O 1s (Non-Lattice)	Zr 3d (Zr-O)	Zr 3d (Zr-C)	C≡C	C-C	C-O	C=O
600s	at. %	65,1	11,54	11,94	5,16	3,1	1,79	0,67	0,69
1200s	at. %	64,51	12,84	11,56	5,29	2,54	1,88	0,64	0,75
1740s	at. %	67,02	10,52	11,62	5,36	2,51	1,86	0,54	0,58

Sample 12A		Non-Lattice	Zr-O	Zr-C				
sputt.time	O 1s	O 1s (Non-Lattice)	Zr 3d (Zr-O)	Zr 3d (Zr-C)	C≡C	C-C	C-O	C=O
600s	67,18	8,76	11,73	5,61	3,64	1,47	0,84	0,77
1200s	66,78	9,15	12,04	5,19	3,42	2,32	0,37	0,74
1740s	67,32	8,08	11,66	5,51	4,07	1,8	0,69	0,87

Fig. 3 Evolution of the principle XPS bands for carbon, oxygen and zirconium along the thickness of irradiated C-doped ZrO_2 films.

3.2. *Analysis of PL maps*

Fig. 4 reports PL maps obtained for pristine zirconia sample (a) and bare fused silica substrate (b), while Fig. I in the Supporting Information (S.I.) gives PLE spectrum. The PL and PLE data show that the visible emission around 450 nm can be activated by three possible transitions as schematically illustrated in Fig. 5 of Ref.[34]: the first one (I) at higher energies (λ_{exc}~200 nm) may be ascribed to $\sigma \rightarrow \sigma^*$ excitation, the second one (II) at λ_{exc}~270 nm corresponds to the $\pi \rightarrow \pi^*$ excitation, while the third one (III) at λ_{exc}~360 nm corresponds to the $n \rightarrow \pi^*$ excitation. For all three transitions, the emission is due to radiative decay from π^* level to n defects levels inside $\pi \rightarrow \pi^*$ gap. For the transition I the radiative decay is accompanied by non-radiative decay from σ^* to π^* level.

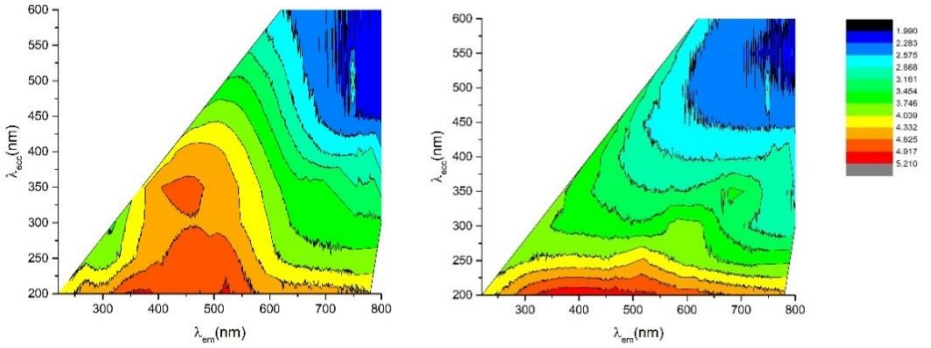

Fig. 4 PL maps for a pristine ZrO_2 film on fused silica (left) and on a bare fused silica substrate (right). The excitation wavelengths and the corresponding emission wavelengths are given on the y and x-axes, respectively.

Fig.5 reports PL maps for irradiated samples together with the element abundance retrieved from the survey spectrum taken at the surface of the irradiated samples. The atomic percentage as a function of the etching time is given for all the irradiated samples in Fig. III of S.I (with 1200 s of etching time corresponding to a penetration depth of 120 nm). As one can note in Fig. 5, the PL intensity ratio of Transition III with respect to Transition I and II increases for the two samples irradiated at higher doses, maybe due to the higher content of carbon partially bonded to oxygen which form n-levels inside π -π* gap. In fact, oxygen content on the surface is very high, giving a ratio with Zr content much higher than the value expected for stoichiometric zirconia (O/Zr=2), especially for samples protonated at higher doses for whom the O/Zr ratio gets values up to 7 and 12. In particular, the ratio between C=O and C-Zr bonds is higher for the irradiated samples as compared to the pristine samples (see Fig. 2 and 3), and it increases with the dose. C=O bonds in carbon materials are known to be responsible for the emission at λ_{em}=450 nm excited at λ_{exc}=300 nm (Transition III) [34]. Therefore, this kind of emission is more intense for high dose-irradiated samples, most probably due to the higher abundance of C=O bonds. The carbon increases on the surface along the radiation dose is due to the build-up of a carbonaceous contamination layer during the irradiation [23]. Although very thin (determined as 0.7 nm for the highest of used fluences [23]) such a layer is sufficiently thick to influence the survey mean values as the information depth of the XPS is approximately 5-10 nm which is comparable with the thickness of the contamination layer rich in carbon.

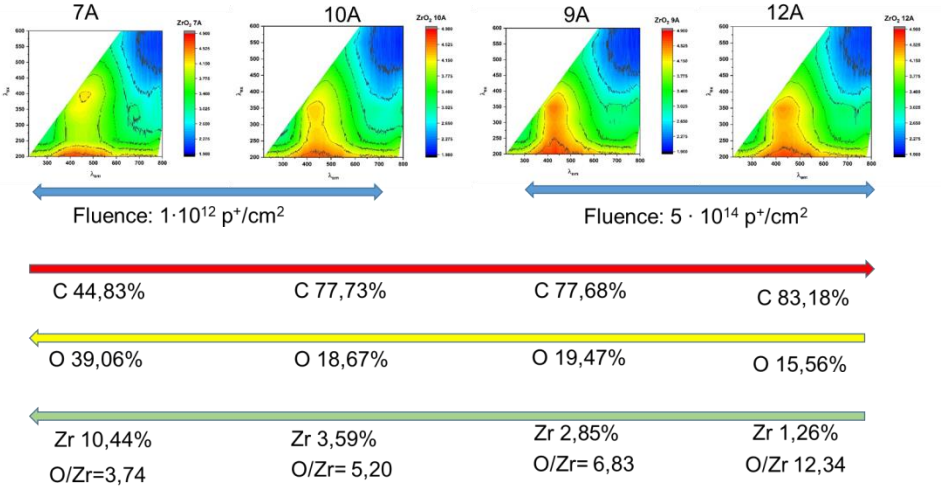

Fig. 5 PL maps for irradiated ZrO_2 films. Modification of the content of carbon, oxygen and zirconium on the films surface due to irradiation.

3.3. *Theoretical simulation of proton-induced damage in C-doped ZrO_2*

In simulating the structural effects of proton irradiation in amorphous C-doped zirconia, the "*Detailed calculation with full damage cascades*" mode in SRIM [35] was employed, and the parameters listed in Tab. 2 were adopted.

Tab. 2 Parameters adopted in the SRIM simulation of 100 keV proton irradiation in C-doped ZrO_2

Atom	Zr	O	C
Stoichiometry	1	2	0.001
Displacement energy (eV)	25	28	28
Lattice Binding Energy (eV)	3	3	3
Surface Binding Energy (eV)	6.33	2	7.41
Mass density (g cm^{-3})		5.68	

It is worth remarking that the reported carbon concentration is defined on a "upper limit" basis, and even in this case the effect of carbon incorporation in the ZrO_2 matrix can be regarded as negligible in terms of the modeled depth profile of the linear density of induced vacancies. From such a profile (reported in Fig. 6) it is possible to estimate the geometrical features summarized in Tab. 3.

Tab. 3 Geometrical ion penetration features for 100 keV protons in carbon-doped zirconia

Direction	Range (nm)	Straggle (nm)
Longitudinal	542	85
Lateral projection	88	112
Radial	138	78

The damage density linearly increases from the film surface towards its depth. This means that the inner part of the film undergoes heavier impact from the radiation. The film material undergoes the structural transformations analyzed in the previous section. The

occurrence of these effects is larger in the upper part of the film due to a higher concentration of impurities. On the other hand, the proton impact increases with the film depth. These two effects induce film densification and lead to a more uniform film. After irradiation, the upper layer rich in impurities becomes much thinner, while the rest of the film is less absorbing [30].

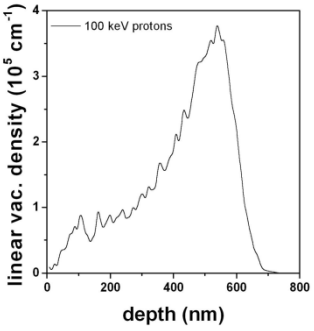

Fig. 6 Linear vacancy density profile induced by 100 keV protons in carbon-doped zirconia

3.4. *Radiation impact on the composition of C-doped zirconia films*

The change of the optical properties for the two types of films was different. Figure 7 compares the transmittance change for the samples 7 and 10 which belong to two different sample types and were irradiated at the same conditions. The induced decrease of transmittance is smaller for sample 10 in the entire investigated spectral range and it is nearly constant, about 2-3%. Instead, for sample 10 the same level of transmittance decrease is observed for the range over 600 nm, while the discrepancy is significantly more pronounced towards the shorter wavelengths, exceeding 5% in the ultraviolet.

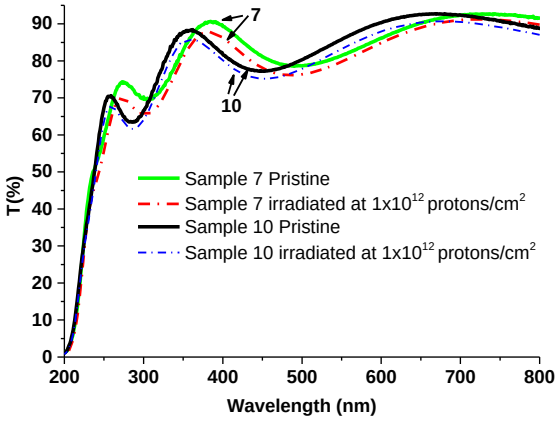

Fig. 7 Transmittance of samples 7 and 10 before and after irradiation.

For some samples, moderate radiation doses produced either no change or even a slight increase in the sample transmittance in the ultraviolet (UV) range. Figure 8 illustrates this effect with an example of the samples 11A and 11B which belong to the same group as sample 10. For the sample 11B which received a dose of 4.5x10^{12} p$^+$/cm^2, the transmittance curve overlaps with that of the pristine sample in the range below 400 nm. For comparison, the insert in Fig. 8 reports the measured spectral transmittance for the uncoated fused silica substrate, for two different irradiation conditions. In the case of fused silica substrate, the damage reduction of the transmittance is well known [36]. For the substrate, the transmittance decrease is present in the entire spectral range and, with the radiation dose increased, the transmittance decay is increasing and more pronounced at shorter wavelengths.

As illustrated in the previous section, the substrates are more affected by the damage induced by 100 keV protons, Fig.6. A fused silica substrate irradiated at the same conditions used for sample 11B loses about 2% of its transmittance due to formation of a ~600nm-thick damaged zone inside the material. This transparency lost is spectrally nearly uniform for the range 200-800 nm. The same value of the transparency decay is kept for sample 11B in the visible and infrared range, while no transmittance decrease occurs in the UV for this sample, as illustrated in Fig.8. Therefore, the unchanged UV-transmittance of sample 11B proves a significant enlargement of the UV transparency of the film materials. In fact, the induced modification within ~190 nm of the film has been sufficient to compensate the decrease of the substrate transparency due to the 600nm-thick absorbing zone formed beneath the substrate surface.

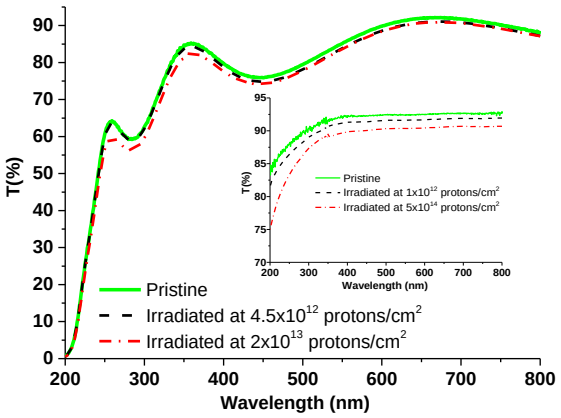

Fig. 8 Transmittance of samples 11A and 11B and of the uncoated fused silica substrate (in insert) before and after irradiation.

The transparency increase in C-doped zirconia films can be explained by reduction of carbon-related absorption. Indeed, thin films of amorphous carbon have a broad band absorption which maximum is positioned in the spectral range of carbon interband transitions 250-350 nm, as illustrated by Fig. 3 in ref. [38]. These transitions have sp3 (diamond-like) and sp2 (graphite-like) characters, but mostly the absorption is determined by strong σ→σ* transitions [39]. Conversely, the reduction of this last transition type upon irradiation has been confirmed by our PL analysis, see below.

The enhancement of the UV transparency of the C-doped zirconia layers due to the impact of energetic particles was confirmed for all the samples by their increased laser-damage threshold values [37].

The reduced carbon content in the irradiated films was evidenced also by the reduction of the C1s-peak area in the XPS survey for the irradiated films compared to pristine ones. For the C1s-peak area estimation, the measurements acquired after etching for dozens of seconds were considered, so that the measurements were not affected by surface adsorption pollution. Thermo's Avantage software used for this calculation takes into account the sensitivity factor for each element.

During the irradiation, the film material may undergo chemical reactions similar to those happening during the ALD growth [e.g. 40] where metal-organic precursor interacts with oxygen and protons when water as co-reactant is used. Such reactions can lead to reduction of the carbon-related absorption. Notice that the non-lattice oxygen abundance in our zirconia films can act as oxidizer source for the completion of the reaction only partially completed during the film growth.

Summarizing, we can state that the XPS depth-resolved investigations revealed the cleavage of Zr-C and of C=O bonds as well as establishment of O-H and C-O bonds (HCO species formation), both increasing towards the film bottom and as the dose increases. The carbonate C=O species (CO_3 complexes attached to Zr atoms) are those responsible for the PL signal (Transition II). The possibly formed C-H bonds may decrease and this effect is more evident for higher radiation doses. Concerning the remaining carbon content, the percentage of carbon bonded to oxygen becomes higher for the samples irradiated at higher dose and this effect induces the increase of PL emission at λ_{em}=450 nm excited at λ_{exc}=300 nm (Transition II) with respect to the emission at λ_{em}=450 nm excited at λ_{exc}=200-270 nm (Transition I).

Fig. 9 gives a comparison between PL maps of each sample before and after irradiation and it is evident that the decrease of emission intensity for all the analyzed irradiated samples. This is due to reduction of carbon-zirconium bonds and decrease of carbon content inside the film upon the irradiation following the reactions (1) and (2). The effect is most pronounced for sample 7A, which indeed has the lowest C=O bond in C1s band after irradiation, Fig.3.

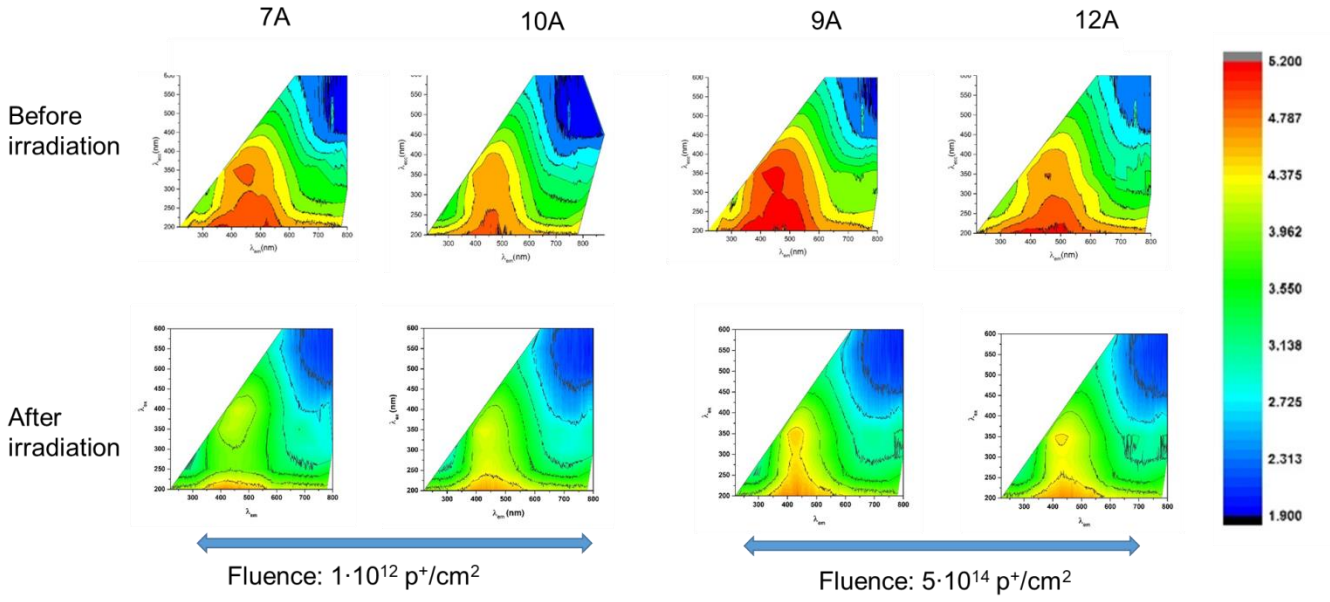

Fig. 9 PL maps for pristine (upper frame) and irradiated (lower frame) ZrO_2 films. Modification of the content of carbon, oxygen and zirconium in the films due to irradiation

4. Conclusions

Amorphous C-doped zirconia thin films obtained using ALD technique on fused silica substrates have high transmittance and significant PL capacity. Carbon doping of zirconia was obtained through incomplete chemical reaction at the last stage of film growth. Due to carbon doping, zirconia films present three main PL transitions: Transition I and II at λ_{em}=450 nm (λ_{exc}=200 and 270 nm), related to sp3 and sp2 C-C bonds, and Transition III at λ_{em}=450 nm (λ_{exc}=300 nm) that can be assigned to C=O bonds which introduce n levels in the π- π* gap.

Since the high transparency of the films in the visible range is preserved by limiting the carbon content, the carbon-doped zirconia may find application as a transparent material to convert high energy into lower energy photons. Moreover, thanks to the substantial change of its optical properties under irradiation, the C-doped zirconia may find application as an optical sensor of radiation. In this study we hence investigated how the PL properties in C-doped zirconia films on silica substrate change under proton radiation. The films underwent low-energy proton irradiation with energy of 100 keV and two values of proton fluences ($1{\cdot}10^{12}$ p⁺/cm² and $5{\cdot}10^{14}$ p⁺/cm²) were used. The changes induced by the radiation in the chemical composition of the films have been monitored as a function of irradiation dose. To this aim, the in-depth resolved XPS analyses have been performed on both the pristine and irradiated samples. The ratio Zr-C/Zr-O bonds decreases under irradiation while the ratio C-H/C-Zr bonds increases, especially at higher doses. Analogously, the ratio C=O/C-Zr bonds increases with respect to pristine samples, especially for high-dose irradiated samples. Therefore, we can conclude that C-Zr bonds are cleaved by protonation in favor of Zr-O, C-H and C=O bonds establishment. As a consequence, more defect levels are formed in the π- π* gap of carbon. Consequently, the emission due to Transitions III becomes more intense for high energy doses, getting intensity values close to Transitions I/II.

Declaration of Competing Interest

The authors declare that they have no known competing financial interests or personal relationships that could have appeared to influence the work reported in this paper.

Data availability

Data may be obtained from the authors upon reasonable request.

Acknowledgments

This work was done with the contribution of the Italian Ministry for University and Research and the Italian Ministry of Foreign Affairs, PGR *AstroOptElect* "Effects of space environment on optical and electronic devices for astrophysical space missions". China-Italy Intergovernmental Cooperation Project under the National Key R&D program of China (2018YFE0118000).

The authors are thankful to Martino Palmisano and Emanuela Pesce from ENEA Brindisi Lab for their technical support in sample characterization.

References

1. Z. Chen, Q. Xu, K. Zhang, W.-H. Wong, D.-L. Zhang, E. Y.-B. Pun and C. Wang, Efficient erbium-doped thin-film lithium niobate waveguide amplifiers, Opt. Lett. 46 (2021) 1161 DOI: 10.1364/OL.420250

2. G. Adamopoulos, S. Thomas , P. Wöbkenberg, D. Bradley, M. McLachlan and T. Anthopoulos, "High-Mobility Low-Voltage ZnO and Li-Doped ZnO Transistors Based on ZrO2 High-k Dielectric Grown by Spray Pyrolysis in Ambient Air", Adv. Mater., 2011, 23 , 1894-1898.

3. D. Clarke and S. Phillpot , "Thermal barrier coating materials", Mater. Today, 8 (2005), 22-29.

4. Hojabri, A. Structural and optical characterization of ZrO2 thin films grown on silicon and quartz substrates. J Theor Appl Phys 10, 219–224 (2016). https://doi.org/10.1007/s40094-016-0218-8

5. M. Jerman, Z. Qiao, and D. Mergel, "Refractive index of thin films of SiO2, ZrO2, and HfO2 as a function of the films' mass density," Appl. Opt. 44, 3006-3012 (2005). https://doi.org/10.1364/AO.44.003006

6. S. Heiroth, R. Ghisleni, T. Lippert, J. Michler, A. Wokaun Optical and mechanical properties of amorphous and crystalline yttria-stabilized zirconia thin films prepared by pulsed laser deposition, Acta Materialia 59 (2011) 2330, https://doi.org/10.1016/j.actamat.2010.12.029

7. J.S. Lakshmi, I. John Berlin, G.P. Daniel, P.V. Thomas, K. Joy, Effect of calcination atmosphere on photoluminescence properties of nanocrystalline ZrO2 thin films prepared by solgel dip coating method, Physica B: Condensed Matter, 406 (2011), 3050. https://doi.org/10.1016/j.physb.2011.05.004

8. M.A. Botzakaki, N. Xanthopoulos, E. Makarona, C. Tsamis, S. Kennou, S. Ladas, S.N. Georga, C.A. Krontiras, ALD deposited ZrO2 ultrathin layers on Si and Ge substrates: A multiple technique characterization, Microelectronic Engineering 112 (2013), 208-212. https://doi.org/10.1016/j.mee.2013.03.002.

9. L. Song, X. Cao, L. Li, "Engineering Stable Surface Oxygen Vacancies on ZrO2 by Hydrogen-Etching Technology: An Efficient Support of Gold Catalysts for Water-Gas Shift Reaction", ACS Applied Materials and Interfaces 10(2018), 31249-

31259

10. S.J. Malode, N.P. Shetti, "ZrO2 in biomedical applications" in Metal Oxides for Biomedical and Biosensor Applications , 2021, p.471-501 DOI: 10.1016/B978-0-12-823033-6.00016-8

11. T. Liu, X. Zhang, X. Wang, et al. "A review of zirconia-based solid electrolytes". Ionics 22 (2016), 2249–2262 https://doi.org/10.1007/s11581-016-1880-1

12. P. Kalita, S. Ghosh, G. Gutierrez, et al. Grain size effect on the radiation damage tolerance of cubic zirconia against simultaneous low and high energy heavy ions: Nano triumphs bulk. Sci Rep 11, 10886 (2021). https://doi.org/10.1038/s41598-021-90214-6

13. K.E. Sickafus, Hj. Matzke, Th. Hartmann, K. Yasuda, J.A. Valdez, P. Chodak, M. Nastasi, R.A. Verrall, "Radiation damage effects in zirconia", Journal of Nuclear Materials, 274 (1999), 66-77, DOI: 10.1016/S0022-3115(99)00041-0

14. V. Ponnilavan, M. Mushtaq Alam, M. Ezhilan, Kalpana Pandian, S. Kannan, "Structural, mechanical, morphological and optical imaging characteristics of Yb3+ substituted zirconia toughened alumina," Materials Today Communications, 24 (2020) 100983, DOI:10.1016/j.mtcomm.2020.100983.

15. K. Smits, L. Grigorjeva, D. Millers, A. Sarakovskis, J. Grabis, W. Lojkowski, Intrinsic defect related luminescence in ZrO2, J. Lumin., 131 (2011) 2058-2062, DOI: 10.1016/j.jlumin.2011.05.018.

16. A. King, R. Singh, R. Anand, S.K. Behera, B.B. Nayak, Phase and luminescence behaviour of Ce-doped zirconia nanopowders for latent fingerprint visualisation, Optik 242 (2021),167087. https://doi.org/10.1016/j.ijleo.2021.167087.

17. Y. Hui, B. Zou, S. Liu, S., Zhao, J. Xu, Y. Zhao, X. Fan, (...), Cao, X., Effects of Eu3+-doping and annealing on structure and fluorescence of zirconia phosphors, Ceramics International, Part PB 41 (2015), 2760-2769. https://doi.org/10.1016/j.ceramint.2014.10.091

18. K. Kobayashi, H. Kuwajima, T. Masaki, Phase change and mechanical properties of ZrO2-Y2O3 solid electrolyte after ageing, Solid State Ionics, 3-4 (1981), 489. doi: 10.1016/0167-2738(81)90138-7

19. R. Di Monte, J. Kašpar, Nanostructured CeO2-ZrO2 mixed oxides, J. Materials Chemistry, 15 (2005), 633. https://doi.org/10.1039/b414244f

20. D.H.A. Besisa, E.M.M. Ewais, Black zirconia composites with enhanced thermal, optical and mechanical performance for solar energy applications, Solar Energy Materials and Solar Cells, 225 (2021), 111063, doi: 10.1016/j.solmat.2021.111063.

21. E. Aleksanyan, M. Kirm, E. Feldbach, K. Kukli, S. Lange, I. Sildos, A. Tamm, Luminescence properties of Er3+ doped zirconia thin films and ZrO2/Er2O3 nanolaminates grown by atomic layer deposition, Optical Materials, 74 (2017), 27-33, DOI: 10.1016/j.optmat.2017.05.003

22. S.V. Nikiforov, A.A. Menshenina, S.F. Konev, The influence of intrinsic and impurity defectsnon the luminescence properties of zirconia, J. Lumin. 212 (2019), 219 https://doi.org/10.1016/j.jlumin.2019.03.062

23. A. Sytchkova, M.L. Protopapa, P. Olivero, L. Tapfer, E. Burresi, T. Dunatov, Z. Siketic, M. Palmisano, E. Pesce, Y. Wang, Z. Wang, H. He, Optical characterization of the impact of 100 keV protons on the optical properties of ZrO_2 films prepared by ALD on fused silica substrates, Appl. Opt. 62(7) 2023, OIC1-OIC5 https://doi.org/10.1364/AO.487523C4.

24. K. Smits, L. Grigorjeva, D. Millers, A. Sarakovskis, J. Grabis, W. Lojkowski, Intrinsic defect related luminescence in ZrO2, J. Lumin. 131 (2011), 2058. https://doi.org/10.1016/j.jlumin.2011.05.018

25. S.V. Nikiforov, A.A. Menshenina, S.F. Konev, The influence of intrinsic and impurity defectsnon the luminescence properties of zirconia, J. Lumin. 212 (2019), 219 https://doi.org/10.1016/j.jlumin.2019.03.062

26. T. Wang, G. Wang, M. Qiu, W. Cheng, J. Zhang, G. Zhao, The origin of the 500 nm luminescence band related to oxygen vacancies in ZrO2, J. Lumin. 237 (2021), 118133, https://doi.org/10.1016/j.jlumin.2021.118133.

27. M. Rushton, I. Ipatova, L. Evitts, W. Lee, S. Middleburgh, Stoichiometry deviation in amorphous zirconium dioxide, RSC Adv., 2019, 9, 16320-16327 https://doi.org/10.1039/C9RA01865D

28. D. Islamov, V. Gritsenko, T. Perevalov, V. Aliev, V. Nadolinny, A. Chin, Oxygen Vacancies in Zirconium Oxide as the Blue Luminescence Centres And Traps Responsible for Charge Transport: Part II - Films. 2020. http://dx.doi.org/10.2139/ssrn.3708728

29. M. Owen, M. Rushton , L. Evitts , A. Claisse, M. Puide, W. Lee, S. Middleburgh, Diffusion in doped and undoped amorphous zirconia, J. Nuclear Materials (2021) 153108. https://doi.org/10.1016/j.jnucmat.2021.153108

30. A. Sytchkova, M. L. Protopapa, P. Olivero, E. Burresi, L. Tapfer, M. Palmisano, E. Pesce, T. Dunatov, Y. Wang, and H. He, "Optical characterization of the impact of 100 keV protons on the optical properties of ZrO_2 films prepared by ALD on fused silica substrates," in Optical Interference Coatings Conference (OIC) 2022, R. Sargent and A. Sytchkova, eds., Technical Digest Series (Optica Publishing Group, 2022), paper WA.2. https://doi.org/10.1364/OIC.2022.WA.2

31. D.A. Shirley," High-Resolution X-Ray Photoemission Spectrum of the Valence Bands of Gold", D. Phys. Rev. B, 5, 4709-4714 (1972). DOI: 10.1103/PhysRevB.5.4709

32. J.H. Scofield, "Hartree-Slater subshell photo-ionisation cross-sections at 1254 and 1487eV", J. Electr. Spectr. Relat. Phenom. 8 (1976) 129–137. DOI: 10.1016/0368-2048(76)80015-1

33. C. Morant, J.M. Sanz, L. Galan, L. Solriano, F, Rueda, " An XPS study of the interaction of oxygen with zirconium", Scurface Science, 218 (1989) 331-345. Doi:10.1016/0039-6028(89)90156-8

34. M.L. Protopapa, E. Burresi, M. Plamisano, E. Pesce, L. Latterini, N. Taurisano, G. Quaglia, R. Mazzaro, V. Morandi, Changing the Microstructural and Chemical Properties of Graphene Oxide Through a Chemical Route, Appl Spectrosc. 76 (2022) 1452-1464. doi: 10.1177/00037028221127048

35 J. F. Ziegler, J. P. Biersack, M. D. Ziegler, "SRIM – The Stopping and Range of Ions in Matter", Mormsville, NC: Ion Implantation Press (2008)

36. I. Di Sarcina, M.L. Grilli, F. Menchini, A. Piegari, S. Scaglione, A. Sytchkova, D. Zola, "Behavior of optical thin-film materials and coatings under proton irradiation", Appl. Opt. 53 (2014) pp.A314-A320. DOI: 10.1364/AO.53.00A314

37. Z. Wang, Y. Wang, H. He, A. Sytchkova, Z. Shen, M. L. Protopapa, Y.Zhang, C. Chen, Y. Chen, Y. Lu, M. Zhu, Y.Shao, J. Shao, "Effect of residual impurities on the behavior and laser-induced damage of oxide coatings exposed to deep space radiation", Optical Materials 140 (2023), 113838. DOI: 10.1016/j.optmat.2023.113838.

38. J. Sancho-Parramon, J. Ferré-Borrull, S. Bosch, A. Krasilnikova (Sytchkova), J. Bulir "New calibration method for UV-vis photothermal deflection spectroscopy set-up", Appl. Surf. Sc, 256 (2006), 158-162. DOI: 10.1016/j.apsusc.2006.06.010.

39. S Logothetidis, "Optical and electronic properties of amorphous carbon materials", Diamond and Related Materials, 12 (2), 2003, 141-150, DOI: 10.1016/S0925-9635(03)00015-3

40. S.T. Barry, "Chemistry of Atomic Layer Deposition", Walter De Gruyter, Berlin-Boston, 2022. DOI: 10.1515/9783110712537

Fig. I. Spectral dispersion of the PL excitation for the emission at λ_{em}=442 nm for pristine samples.

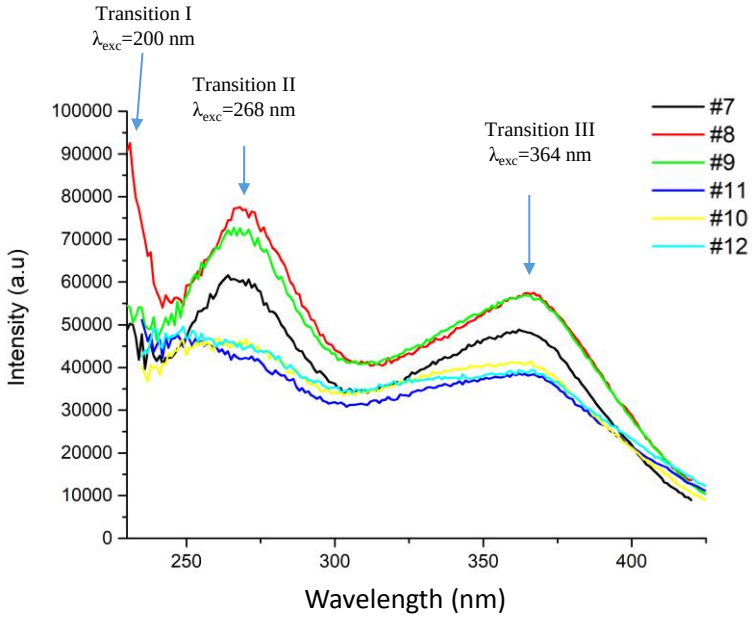

Fig. II. XPS analyses: Atomic percentage as a function of etching time for the irradiated sample

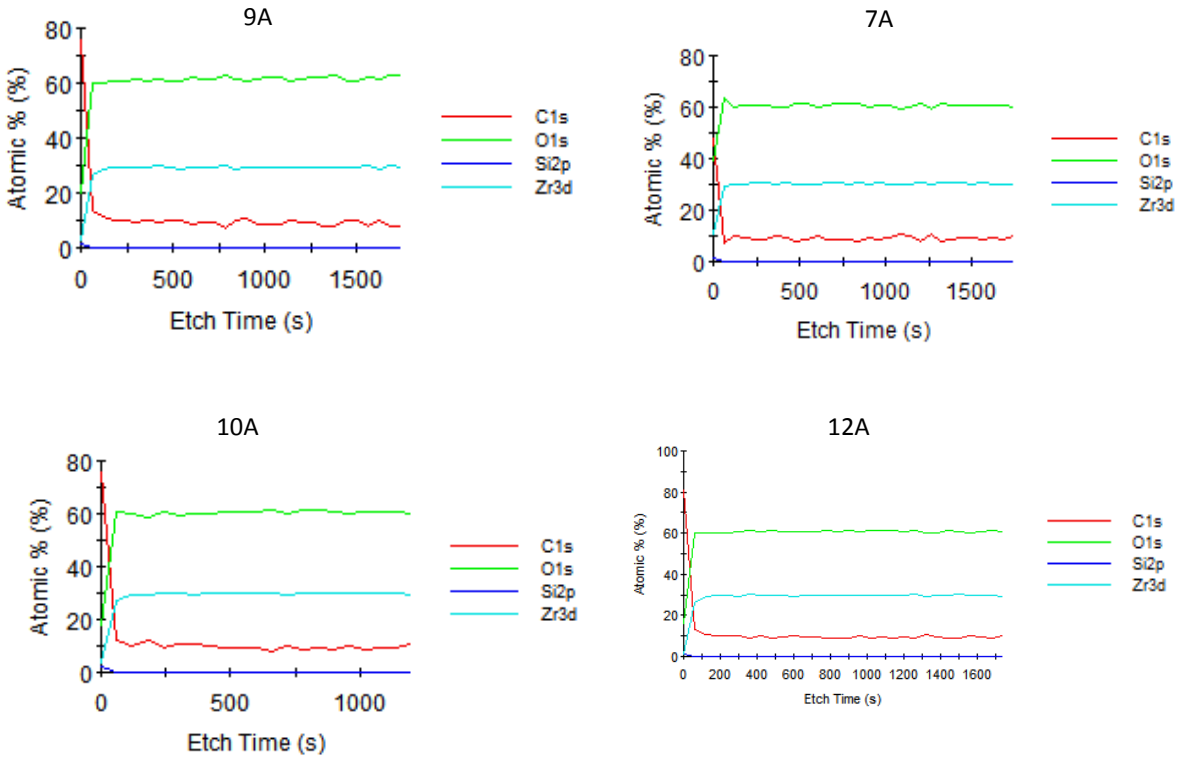

Graphical abstract

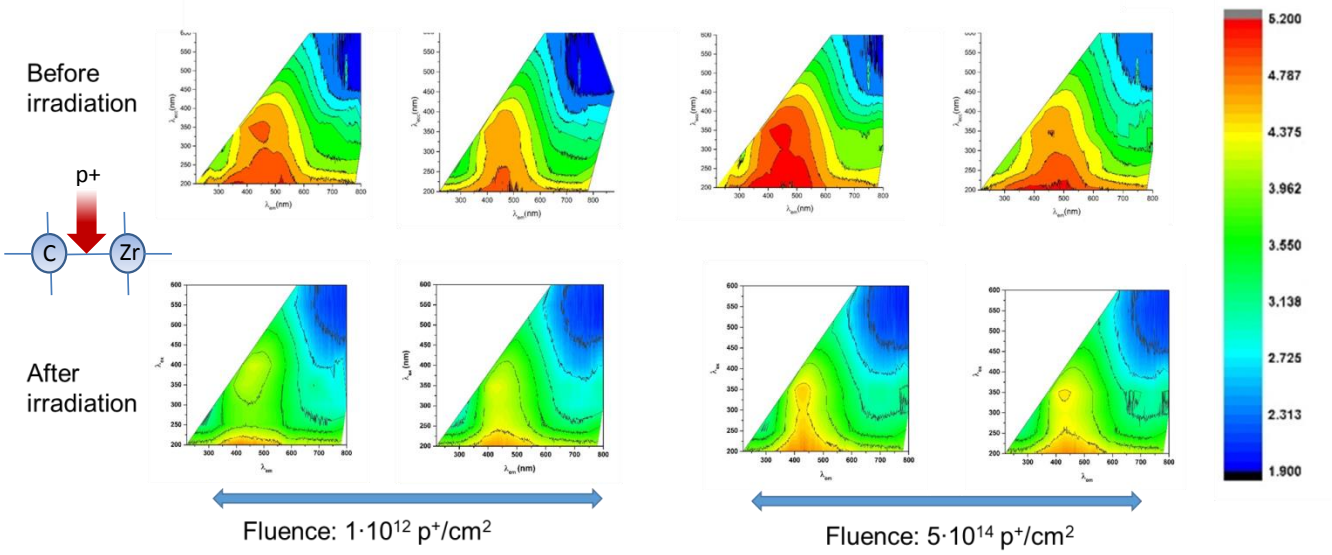

Graphical Abstract (for review)

Click here to access/download;Graphical Abstract (for review);Graphical abstract 10.08.docx

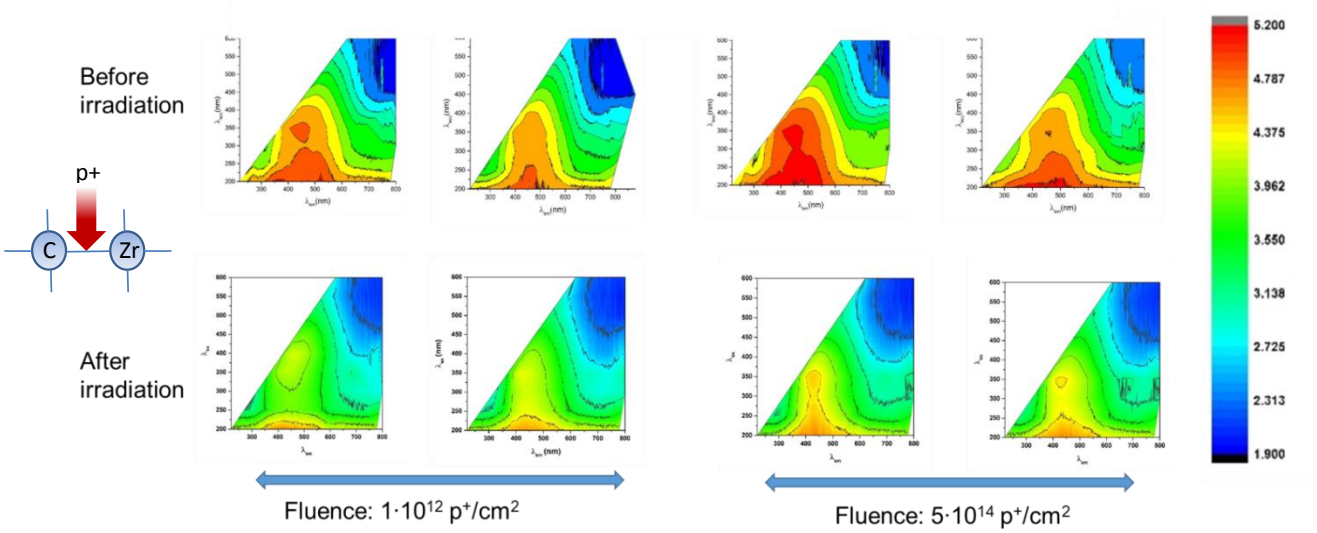

Declaration of interests

☒The authors declare that they have no known competing financial interests or personal relationships that could have appeared to influence the work reported in this paper.

☐The authors declare the following financial interests/personal relationships which may be considered as potential competing interests:

Highlights

- investigation on the composition and PL ability of C-doped a-ZrO_2 films;
- systematical study of the impact of low-energy protons on C-doped zirconia films' composition and PL ability;
- XPS and PL spectroscopic analysis;
- possible applications in dosimetry and radiation imaging.

Dear Prof. Guido Grundmeier,

We would like to thank you as well as the Reviewers for investing time in considering and reviewing our manuscript entitled “Impact of proton irradiation on photoluminescent properties of C-doped ZrO_2 films prepared by ALD” manuscript APSUSC-S-22-24997. All the comments received have been carefully considered and addressed; as a result, significant changes have been made to the manuscript and supplemental document. In particular, we have added substantially more experimental data and further analysis:

- Surface morphology - SEM images.
- More details on the doping origin.
- Ellipsometric investigation on the film inhomogeneity and dopant in-depth distribution.
- XPS analysis data has been re-elaborated.

We are confident that these changes have improved our work and hope the Editor and Reviewers find the revised material satisfactory and would like to resubmit the paper in its new version.

The present manuscript has not been published nor is under review elsewhere. All authors have approved the revised materials and declare no conflicts of interest. Thank you for your consideration.

Best regards,

Anna Sytchkova, on behalf of co-authors.